IOP Publishing Physics in Medicine and Biology

Phys. Med. Biol. **52** (2007) 4189–4204 doi:10.1088/0031-9155/52/14/011

Model for the ultrasound reflection from micro-beads and cells distributed in layers on a uniform surface

O Couture, E Cherin and F S Foster

Imaging Research, Sunnybrook Health Sciences Centre/University of Toronto, Toronto, Canada

E-mail: olicou@swri.ca

Received 12 February 2007, in final form 11 May 2007
Published 15 June 2007
Online at stacks.iop.org/PMB/52/4189

Abstract

A model predicting the reflection of ultrasound from multiple layers of small scattering spheres is developed. Predictions of the reflection coefficient, which takes into account the interferences between the different sphere layers, are compared to measurements performed in the 10–80 MHz and 15–35 MHz frequency range with layers of glass beads and spherical acute myeloid leukemia (AML) cells, respectively. For both types of scatterers, the reflection coefficient increases as a function of their density on the surface for less than three superimposed layers, at which point it saturates at 0.38 for glass beads and 0.02 for AML cells. Above three layers, oscillations of the reflection coefficient due to constructive or destructive interference between layers are observed experimentally and are accurately predicted by the model. The use of such a model could lead to a better understanding of the structures observed in layered tissue images.

(Some figures in this article are in colour only in the electronic version)

1. Introduction

The reflection from interfaces and backscattering from tissues or contrast agents have been extensively studied and sometimes modeled (Sleefe and Lele 1988, Shung and Thieme 1993, Insana *et al* 1990). In general, the reflection of ultrasound from structures depends on the difference in acoustical properties (density, compressibility) between the structure and of the surrounding medium, but also on its size and geometry.

Layered structures are of particular importance in ultrasound. Many tissues, such as epithelia, are stratified, and although their appearance on ultrasound images has been well documented, it is sometimes poorly explained and subject to controversy. The origin of each reflection from the wall of the stomach, for example, has been the subject of debate (Bolondi *et al* 1986, Lim and Jeong 1994). In this tissue, it is often difficult to determine whether the various hypoechoic and hyperechoic regions observed in ultrasound images correspond to real

layers or the difference in aspect is produced by some phenomenon of localized interference. Similar concerns have been raised about human arteries (Siegel *et al* 1993). The complexity of the echo originates mainly from the fact that the different structures forming these tissues cannot be resolved in space, and also that their appearances change with the frequency used. Therefore, it is of particular interest to develop a model able to predict the interference in layered structures, which is applicable at all frequencies.

Previous work in our laboratory has concentrated on the physics behind the reflection enhancement when contrast agents are bound to a surface (Couture *et al* 2006). Our studies have demonstrated that, when particles of liquid perfluorocarbon are deposited on a surface, the reflection coefficient increases linearly with the density of the particles on the surface. However, at a specific density, the reflection coefficient saturates. In the case of glass beads, we also demonstrated that the reflection coefficient decreases with further accumulation of beads.

The goal of this study is to explain the saturation of the signal when several layers of micro-beads or cells are accumulated on a surface. For particles with scattering cross-section much lower than their geometric cross-section, it is hypothesized that the signal saturation is caused by interference between layers. This paper consists of three parts: the development of the interference model, its validation by comparison with experiments performed with layers of glass beads and its application to layers of cells.

2. Theoretical method

The coefficient of reflection from several layers of homogenous materials is derived in most optics or ultrasound books (Cobbold 2007). The approach of considering tissues as multiple layers of homogenous media of known acoustical properties has already been discussed for particular ultrasound applications (Hughes *et al* 1999, Chivers and Santosa 1986), and has also been applied to contrast agents (Lanza *et al* 1998). Here, we discuss the case where the scattering cross-section of each particle forming the layer, rather than the acoustical impedance of the layer itself, is known.

The objective of our work is to estimate the reflection coefficient due to several layers of particles. Our model is based on the hypothesis that it can be calculated by summing the reflection coefficient of individual layers after proper consideration of the phase-shift which is based on the thickness of the layers and the speed of sound. It has been shown in Couture *et al* (2006) that the reflection coefficient of a single layer can be determined from the linear sum of the backscattering cross-sections of each particle.

As shown in figure 1, describing the model, the particles are spherical with a radius of a. In the horizontal plane, it is assumed that they accumulate over the underlying surface until no particle may be moved to create holes sufficiently large for additional particles and in a configuration without any short- or long-range order. Based on numerical calculations performed by Hinrichen *et al* (1990) on the random packing of discs in two dimensions, the coverage fraction is expected to be 0.8 for a single layer. In the vertical direction, it is assumed that the spheres are stacking in a hexagonal pattern with a minimum inter-plane distance of $a\sqrt{2}$. The maximum surface density of the particles is determined from their diameter, and their individual backscattering cross-section is calculated from their size and composition using the Faran model (Faran 1951). The Faran model, which is applicable for fluid or solid particles, can also be used to describe the scattering of cells (Baddour *et al* 2005).

The reflected amplitude from multiple layers of particles can be determined with a recursive formula relating the reflection from N layers to the reflection from $N-1$ layers. The total reflected pressure from N layers is the pressure reflected from the top layer added to the

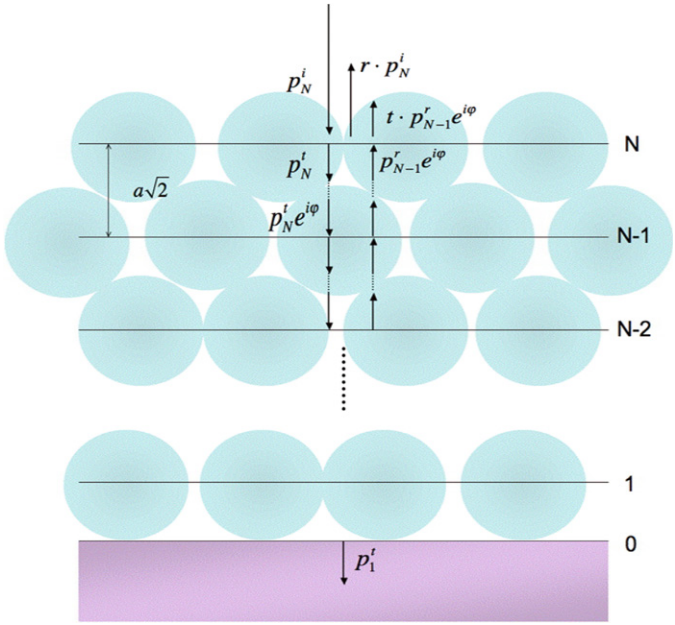

Figure 1. Schematic representation of the layer model. The particles are lying randomly in the horizontal plane, but are organized hexagonally in the vertical direction. The radius of spheres a determines the inter-plane distance.

pressure reflected from $N-1$ underlying interfaces, which is modulated by the transmission coefficient through the top layer and phase shifted by an angle φ related to the layer thickness and speed of sound:

$$p_N^r = t_S \cdot p_{N-1}^r \cdot \exp(-\mathrm{i}\varphi) + r_S \cdot p_N^i, \tag{1}$$

where p_N^i is the incident amplitude at interface N, p_N^r is the reflected amplitude at interface N, p_{N-1}^r is the reflected amplitude at the interface $N-1$, r_S is the reflection coefficient of a single layer, and t_S, its transmission coefficient. Note that the reflection and transmission coefficients are assumed to be equal in both vertical directions. The reflected pressure at the interface $N-1$ is the incident pressure at the interface $N-1$ multiplied by the equivalent reflection coefficient of all layers underneath (r_{N-1}):

$$p_N^r = t_S \cdot r_{N-1} \cdot p_{N-1}^i \cdot \exp(-\mathrm{i}\varphi) + r_S \cdot p_N^i. \tag{2}$$

The incident pressure at the interface $N-1$ is the phase-shifted transmitted pressure through the interface N.

$$p_N^r = t_S \cdot r_{N-1} \cdot p_N^i \cdot \exp(-\mathrm{i}\varphi) \cdot t_S \cdot \exp(-\mathrm{i}\varphi) + r_S \cdot p_N^i. \tag{3}$$

The reflection coefficient of N layers is then obtained by calculating the ratio of the reflected pressure to the incident pressure:

$$r_N \equiv \frac{p_N^r}{p_N^i} = t_S^2 \cdot r_{N-1} \cdot \exp(-2\mathrm{i}\varphi) + r_S. \tag{4}$$

The phase shift depends on the thickness of the layer ($a\sqrt{2}$), the wavelength (c/f) of the wave inside the slab of particles and the attenuation ($\alpha(f)$). The attenuation in each layer is expressed by adding an imaginary component in the phase-shift term. By inspection

$$\varphi = 2\pi \frac{f}{c}\sqrt{2}a - \mathrm{i}\alpha(f) \cdot \sqrt{2}a. \tag{5}$$

Combining equations (4) and (5)

$$r_N = t_S^2 \cdot r_{N-1} \cdot \exp\left(-2\mathrm{i}\left(2\pi \frac{f}{c}\sqrt{2}a - \mathrm{i}\alpha(f)\sqrt{2}a\right)\right) + r_S. \tag{6}$$

Due to the principle of conservation of energy, the amplitude transmission coefficient t_S is related to the amplitude reflection coefficient r_S by $t_S^2 = 1 - r_S^2$. The expression of the coefficient of reflection from N layers of particles can therefore be expressed as a function of the coefficient of reflection from $N-1$ layers, recursively:

$$r_N = r_{N-1} \cdot \Lambda + r_S, \tag{7}$$

where $\Lambda = \left(1 - r_S^2\right) \cdot \exp\left(-2\mathrm{i}\left(2\pi \frac{f}{c}\sqrt{2}a - \mathrm{i}\alpha(f)\sqrt{2}a\right)\right)$. Being recursive, equation (7) allows each layer to have a different reflection coefficient. The underlying surface can also be treated as an additional layer. If the reflection coefficient of the underlying surface (r_0) is assumed to be 0 and the reflection of all other layers is assumed to be r_S, equation (7) can be rewritten as a sum of polynomials:

$$r_N = r_S \cdot \sum_{j=0}^{N-1} \Lambda^j. \tag{8}$$

Using the properties of infinite series, it is possible to obtain an analytical expression:

$$r_N = r_S \cdot \left(\frac{1 - \Lambda^N}{1 - \Lambda}\right). \tag{9}$$

Equation (9) represents a function oscillating with a period dependent on the frequency of the incident pulse, the size of the scatterers and the number of layers. The position of the first maximum of the function can be determined by

$$N = \frac{c}{4\sqrt{2}af}. \tag{10}$$

The reflection coefficient of a single layer of particles (r_S), which is used in these formulae, can be estimated from a model developed for low concentrations of particles deposited on a poorly reflective surface. This model calculates the reflection coefficient based on the sum of the differential backscattering cross-section of particles weighted by the diffraction pattern of the transducer. The contribution from the particles is then simply added linearly to the reflection from the surface. c and $\alpha(f)$ are properties of the medium comprising the particles and the interstitial fluid. These parameters can either be determined experimentally or using theoretical models. For the glass bead case, we used the values of speed of sound and attenuation reported by Williams *et al* (2002) for layers of sand in the sea, which were estimated using a model developed by Buckingham (1997). When these models are adapted to Pyrex glass, the speed of sound is predicted to be 1860 m s^{-1} and the attenuation coefficient to be 5.3 dB mm^{-1} at 40 MHz.

3. Experimental method

3.1. Glass beads

The experiment involving micro-beads was described in detail in Couture *et al* (2006). In brief, 5.1 μm diameter glass beads were accumulated on a poorly reflective surface made of Aqualene, a rubber of acoustical impedance very close to water (figure 2). The resulting change in reflected signal was measured with a 40 MHz transducer (12 mm focal length, 3 mm aperture) emitting pulses (−6 dB bandwidth: 3 MHz) at various frequencies covering

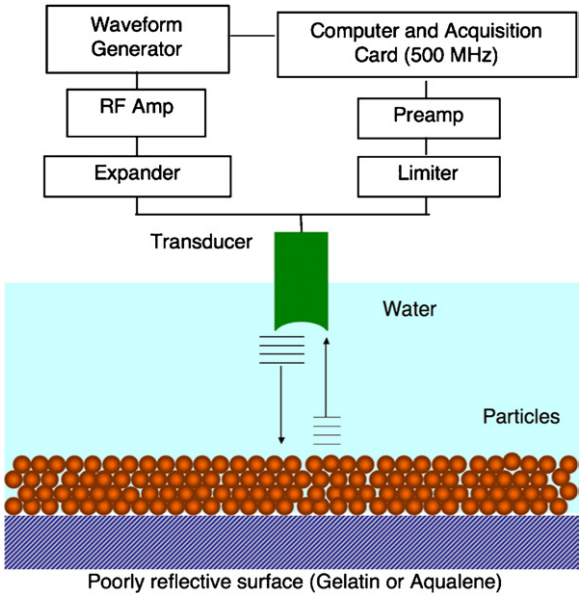

Figure 2. Data acquisition setup for the determination of the reflection coefficient of multiple layers of micro-beads. For the experiment on cells, the electronics are replaced by a Visualsonics Vevo 770 system.

the range from 10 to 80 MHz. The peak-negative pressure at the focus was measured to be −0.79 MPa. Previous experiments have shown that such pressures do not affect the glass beads in terms of motion due to radiation pressure.

Reflection coefficients were obtained by comparing the amplitude of the reflected signal with that from a quartz flat. The reflection coefficient from the underlying surface was subtracted from the reflection coefficient of the surface covered by the glass beads. The surface density of the micro-beads was calculated from their total mass, density and radius. The number of layers of these beads was then determined on the basis that loose-random packing of discs yields a surface coverage fraction of 0.8.

3.2. AML cells

Acute myeloid leukemia (AML) cells were cultured in a minimum essential medium. The cells were centrifuged, transferred into phosphate buffered saline (PBS) and counted with a hemocytometer. The cells were then diluted at different concentrations in PBS and kept at 4 °C for the duration of the experiments.

A solution of 2% w/v of gelatin (300 Bloom, Sigma Inc., Saint-Louis, USA) was poured in a tissue culture dish. After solidification, a square grid was put over the surface to compartmentalize the surface of gelatin. Each of the compartments was then filled with 200 μl of one of the dilutions of AML cells. The same dilutions were also poured into a 96-well plate with a clear bottom (Corning Incorporated, Corning, NY, USA). Both gelatin and 96-well plates were then left undisturbed for 70 min for the cells to deposit on the surface.

Ultrasound scans of the gelatin surface with AML cells were performed using a Visualsonics Vevo770 (Visualsonics, Toronto, Canada) equipped with a 30 MHz probe (model RMV 707, 12.7 mm focal length, 6 mm aperture). The probe was positioned such that

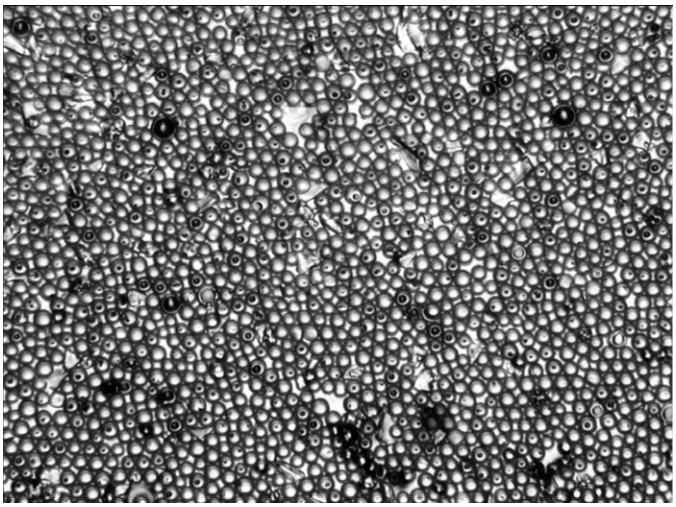

Figure 3. Bright-field microscope image (400×) of loosely packed glass micro-beads. The beads are 5.1 μm in diameter.

the transducer was focused on the surface. Single cycle pulses at 277 kPa peak-negative pressure were used to obtain 3D images with a field of view of 7 mm × 7 mm centered over the compartment containing AML cells. RF data were also acquired by an A/D card at a sampling rate of 500 MHz (DP240, Acquiris, Geneva, Switzerland) and later analyzed with Matlab (The Mathworks, Natick, MA, USA). The reflection coefficient was obtained by comparing, in the frequency domain, the amplitude of the echo reflected from a surface covered with AML cells to the amplitude of the echo reflected from a quartz flat (reflection coefficient 0.79). The reflection coefficient was then averaged between uncorrelated regions of the surface to account for the different conformations taken by the scatterers. The experiments were performed for 24 different densities of AML cells on the surface, ranging from 0 to 2.8×10^{10} cell m^{-2} (or 10.4 layers). Each experiment was repeated four times to derive uncertainties.

In parallel to the ultrasound scans, images of the cells in the 96-well plate were collected using a bright-field microscope (Leica, Wetzlar, Germany), at a magnification of 100× for counting, and a magnification of 400× for sizing.

4. Results

4.1. Glass beads

Figure 3 shows an optical microscope image of the glass beads used in these experiments. In this particular image, the glass beads are close to confluence, distributed randomly over the surface, occupying most of it.

As shown in figure 4, the reflection coefficient increases with frequency when a single layer of glass beads is covering the surface. Fundamentally, this reflection coefficient is the sum of the scattering cross-section of 3.9×10^{10} particles m^{-2} weighted by diffraction. The theoretical values were calculated independently from the experimental data. In this particular case, no interference between multiple layers is present. Consequently, the theoretical curve follows the prediction of the model for particles at low surface as demonstrated in Couture *et al* (2006).

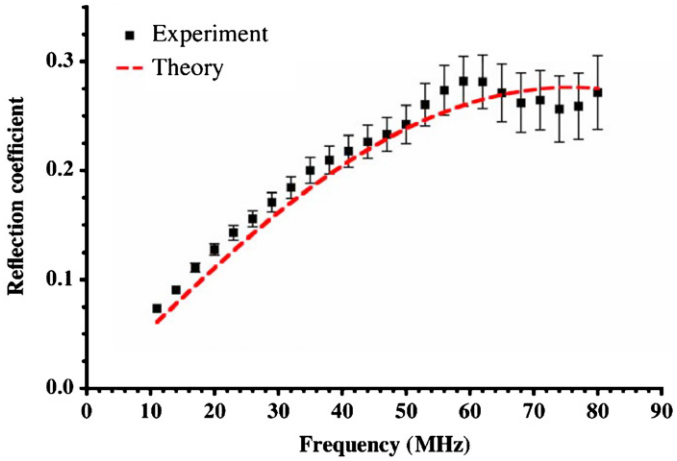

Figure 4. Frequency dependence of the reflection coefficient of a surface covered with a single confluent layer of glass beads. Standard deviations shown ($n = 10$).

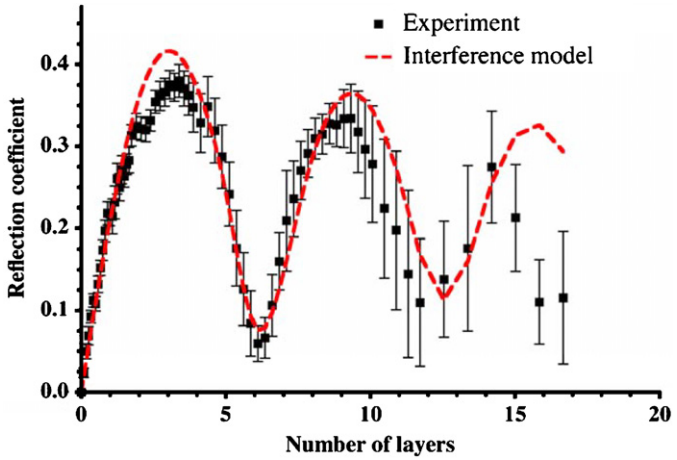

Figure 5. Reflection coefficient from a surface covered with an increasing number of layers of glass beads. The model is calculated from equation (7), with the reflection coefficient of a single layer calculated directly from the theoretical differential backscattering cross-section of glass beads. The error bars represent the standard deviations over trials performed on different regions of the surface ($n = 10$).

The influence of the surface density of glass beads on the reflectivity of the surface at 40 MHz is presented in figure 5. In the experimental data, the reflection of the underlying surface (Aqualene) has been subtracted from the subsequent measurement of reflectivity of glass beads and, consequently, the reflection coefficient of layer 0 is 0. Surface densities are presented as a number of layers. A fractional number of layers represents the ratio between the number of cells on the surface and the number of cells required for them to be confluent in a random-loose arrangement. At this frequency, the increase in the reflection coefficient was found to be linear for values less than one layer ($R^2 = 0.988$, slope $= 0.221 \pm 0.007$, y-intercept: 0.009 ± 0.004). The reflection coefficient increases until reaching a maximum at 3.4 layers ($r_c = 0.38$) and then oscillates, with minima at 6.1 layers ($r_c = 0.06$) and 11.7 layers

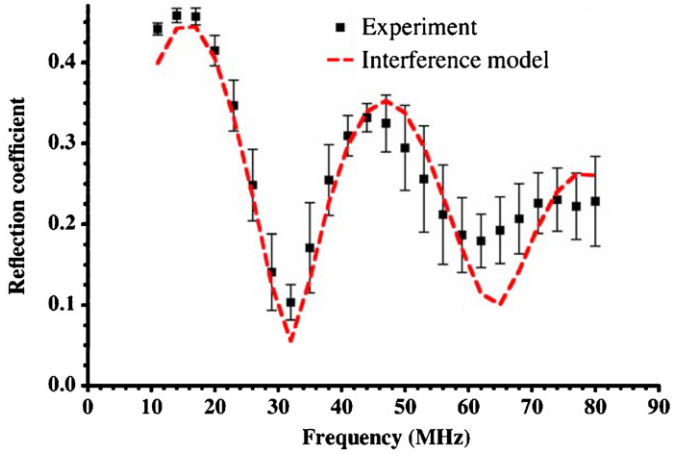

Figure 6. Frequency dependence of the reflection coefficient of a surface covered with the equivalent of eight confluent layers of glass beads. Standard deviations shown ($n = 10$).

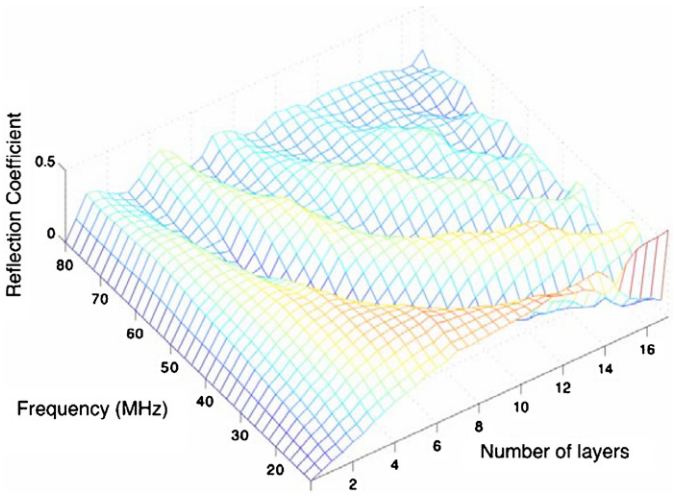

Figure 7. Oscillations in the measured averaged reflection coefficient for an increasing number of layers of glass beads at various frequencies.

($r_c = 0.11$), and maxima at 9.1 layers ($r_c = 0.33$) and 14.2 layers ($r_c = 0.27$). The amplitude of the maxima and minima decreases with the number of layers.

In general, the interference model follows accurately the oscillations in figure 5. The maximum reflection coefficient is overestimated by the model ($r_{c\,\mathrm{theory}} = 0.42$ as compared to $r_{c\,\mathrm{expt}} = 0.38 \pm 0.02$). The distance between the first two maxima is also slightly overestimated by the model, predicted to be 6.4 layers as compared 5.7 layers experimentally. The interference model deviation from experimental data increases with surface density.

Further evidence of interference can be found for the reflection coefficient of eight layers of glass beads (figure 6) which oscillates with maxima at 14 MHz ($r_c = 0.46$) and 47 MHz ($r_c = 0.32$), and minima at 32 MHz ($r_c = 0.10$) and 62 MHz ($r_c = 0.18$). The interference model accurately predicts these fluctuations.

Oscillations in the averaged reflection coefficient over all frequencies and surface densities studied are presented in figure 7. Observations about interference phenomena in figures 4–6

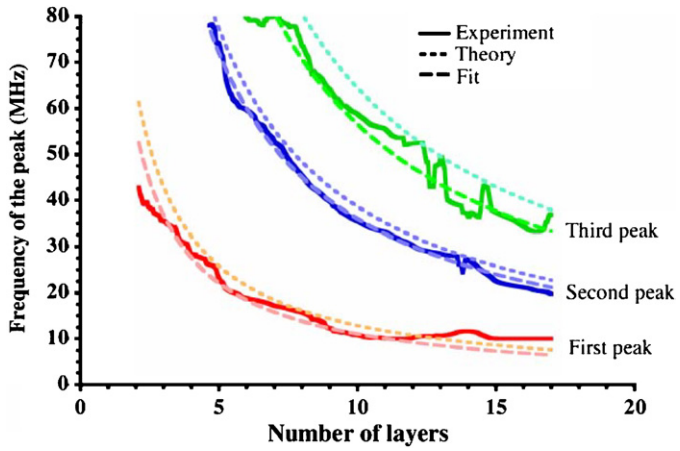

Figure 8. Experimental and theoretical position of the peak reflectivity in figure 7.

can be generalized. Experimental measurements and model predictions are in good agreement in the 10–80 MHz frequency range for a number of layers ranging from 0 to 16.7 ($X^2 = 4.6$, $R^2 = 0.85$). For a frequency range reduced to 30 to 50 MHz and a number of layers ranging from 0 to 10 layers, the agreement between the model and the experiment is improved ($X^2 = 3.1$, $R^2 = 0.93$).

The frequencies at which the first, second and third peaks of the interference pattern are found depend on the number of layers, as shown in figure 8. The theoretical values are determined from equation (10) for a speed of sound of 1860 m s^{-1} and a glass bead diameter of 5.1 μm. For the first peak, the correlation between the experimental and theoretical values is $R^2 = 0.79$. Equation (10) can also be fitted to experimental values in order to find, independently, the ratio between the speed of sound and the size of the particles. The fits for the first peak ($R^2 = 0.92$) and the second peak ($R^2 = 0.99$) yield a ratio $c/a = 6.2 \times 10^8$ s^{-1} and 6.8×10^8 s^{-1}, respectively. For glass beads 5.1 μm in diameter, this would produce a speed of sound of 1600 m s^{-1} or 1731 m s^{-1}.

4.2. AML cells

Two microscope pictures of sparse populations of AML cells are shown at two different magnifications in figure 9. From this picture, the surface density was calculated to be 1330 cells mm^{-2}. On the magnified picture in figure 9, which is one of the seven pictures used to determine the size of the cells, most cells appeared to be spherical. However, some cells seemed to have some vacuoles on their surface. The size distribution of the cells is presented in figure 10. A total of 350 cells were counted and their diameters were determined to be Gaussian distributed ($R^2 = 0.99$) with a mean and standard deviation of 9.77 μm and 1.86 μm, respectively. The density of cells at the surface was measured, in the low end, from the microscope picture obtained at 100× magnification. Figure 11 shows that the surface density of cells increases linearly ($R^2 = 0.998$) with the number of cells added originally in the solution (slope: $(112 \pm 3) \times 10^3$ cell mm^{-2}, intercept: -50 ± 90 cell mm^{-2}). The conversion between cell surface density and number of layers is also shown in this graph. It is based on the average surface area of AML cells as determined in figure 10. For higher concentrations of cells in the original solution, the surface density is assumed to stay linear since the cell

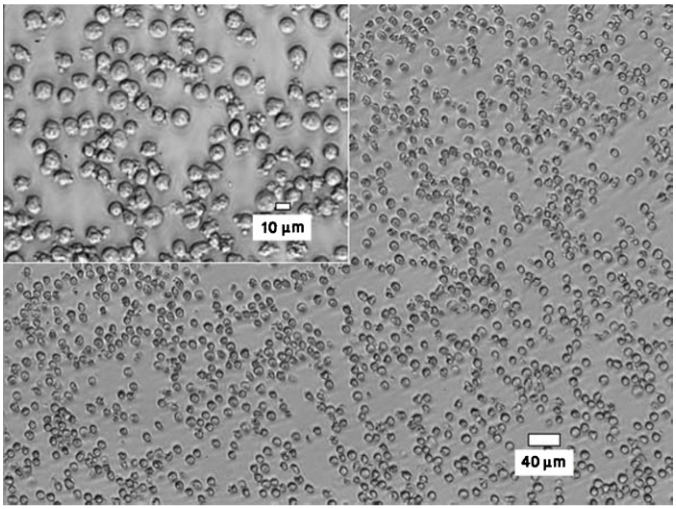

Figure 9. Bright-field microscope images (100× and 400×) of AML cells on the surface of a 96-well plate. The image has been histogram equalized.

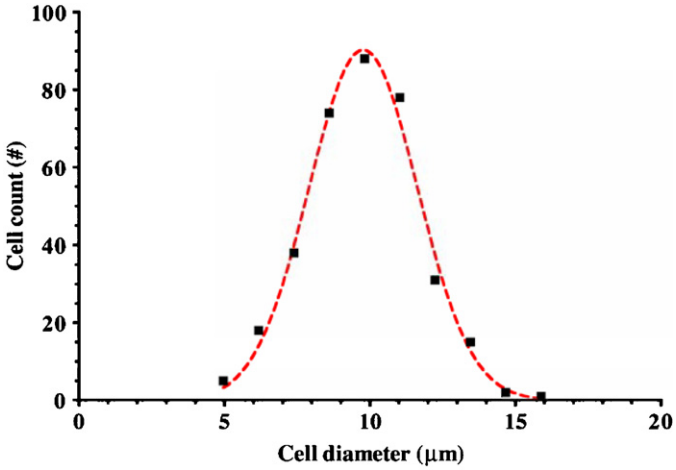

Figure 10. Size distribution of AML cells as measured on microscopy images. The distribution is Gaussian distributed ($R^2 = 0.99$) with a mean and standard deviation of 9.77 μm and 1.86 μm, respectively.

number is conserved. However, the error in this prediction from the linear fit increases with surface density.

The increase of the reflection coefficient at 30 MHz as a function of the number of AML cells on the surface is shown in figure 12. In contrast to the glass beads, the reflection coefficient from the underlying surface could not be subtracted from the reflection coefficient of the measurements with overlying cells, because the reflection coefficient of the cell covered surface did not increase linearly with the number of deposited cells even at the lowest densities. Consequently, the underlying surface had to be calculated has an additional layer in equation (7). The reflection coefficient reaches a maximum for 2.5 layers ($r_c = 0.021$), and appears to reach a minimum for 4.1 layers ($r_c = 0.016$). At higher surface densities

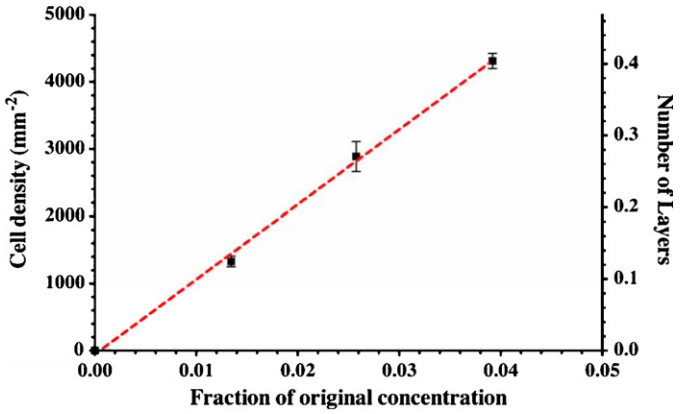

Figure 11. Surface density of deposited AML cells obtained from different volume concentrations of cells. The original concentration is an arbitrary number representing the maximum volume concentration of cells used. The surface density could only be determined for low concentrations. The increase in surface density is linear ($R^2 = 0.998$) with respect to volume concentration with a slope of $(112 \pm 3) \times 10^3$ cell mm^{-2} and a y-intercept of -50 ± 90 cell mm^{-2}. Standard deviations shown.

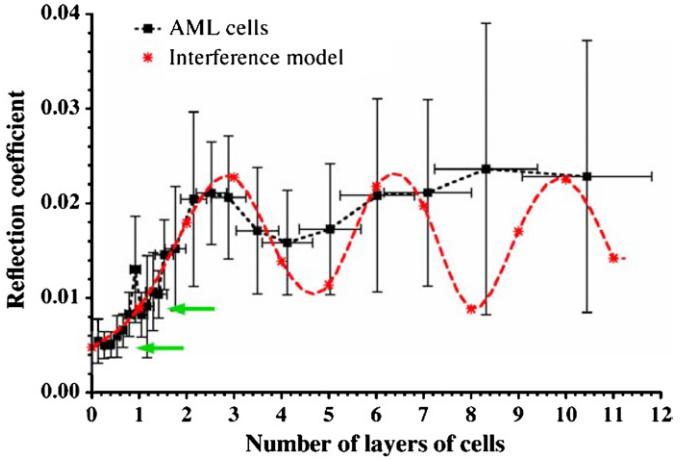

Figure 12. Reflectivity, at 30 MHz, of a surface covered with an increasing number of layers of AML cells. The interference model is calculated from equation (8) with the reflection coefficient of a single layer determined experimentally from a fit of the data within two layers (first arrow, 0 layer; second arrow, 1 layer). Standard deviations shown ($n = 4$).

the reflection coefficient varied considerably with a relatively constant mean. As shown in figure 13, the reflection coefficient of three layers actually decreases with frequency. The reflection coefficient at ten layers also decreases, although with a more pronounced slope (figure 14).

In contrast to the glass beads, for which the model was purely theoretical, some parameters determined experimentally had to be used for the modeling of AML cells. The speed of sound ($c = 1461$ m s^{-1}) and the attenuation coefficient ($a = 0.012 f^{1.48}$ dB mm^{-1}) in the mix of AML cells and PBS were determined experimentally in pellets of cells at 4 °C. The reflection coefficients R_0 and R_1 of the 0th and the 1st layers were determined from a second-order fit of the experimental values from 0 to 1.4 layers. At 30 MHz, they are 0.005 and 0.009,

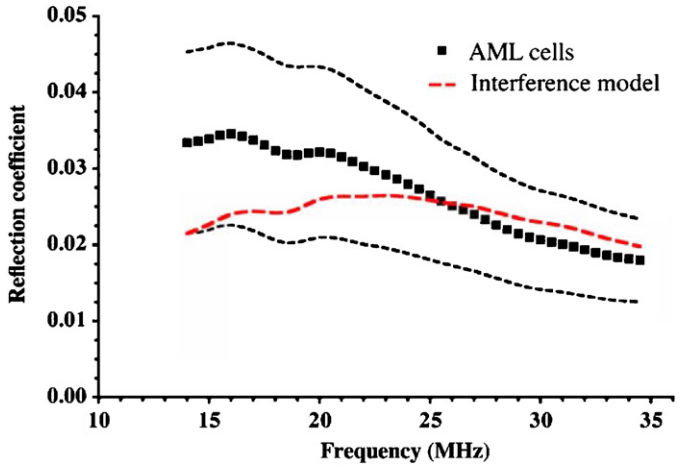

Figure 13. Frequency dependence of the reflectivity of a surface covered with three confluent layers of AML cells. Standard deviations shown ($n = 4$).

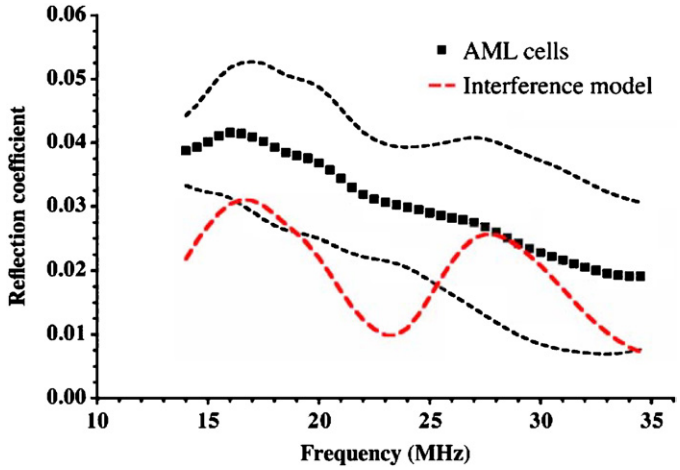

Figure 14. Frequency dependence of the reflectivity of a surface covered with ten confluent layers of AML cells. Standard deviations shown ($n = 4$).

respectively. Then, the interference model was used to extrapolate the reflection coefficient of multiple layers of AML cells.

The model prediction for the maximum reflection coefficient ($r_c = 0.023$) was within the error of the experimental value ($r_c = 0.020 \pm 0.005$). The model also predicted a minimum between 4 and 5 layers of AML cells. The reflection coefficient oscillated with a period of 3.5 layers, which is identical to the value obtained with equation (10). The amplitude of the oscillations predicted by the model was more pronounced than the amplitude observed in experimental measurements. Experimental measurements and model predictions are in good agreement in the 15–35 MHz frequency range for a number of layers ranging from 0 to 10 ($X^2 = 3.4$, $R^2 = 0.89$).

Previously, the reflection coefficient for one layer of glass beads was calculated from its theoretical differential backscattering cross-section and the diffraction pattern of the transducer. It was consequently possible to do the inverse analysis. The experimental backscattering

cross-section can be obtained by dividing the reflection coefficient of a single layer by the corresponding number of cells and the correction for the diffraction of the transducer. The measured differential backscattering cross-section of AML cells increases from $(1.2 \pm 0.4) \times 10^{-16}$ m^2 Sr^{-1} at 14 MHz to $(1.2 \pm 0.7) \times 10^{-15}$ m^2 Sr^{-1} at 35 MHz. These values are significantly smaller than theoretical predictions from the Faran model using published acoustical properties of cells (Baddour *et al* 2005).

5. Discussion

When small numbers of particles are present on a surface, the ultrasound reflection coefficients of both types of particles behave similarly. The increase in reflectivity with the surface density was already described and modeled in Couture *et al* (2006). In this regime, the reflection coefficient is simply the sum of the backscattering cross-section of the particles weighted by the frequency-dependent diffraction. The reflection coefficient of one layer of glass beads can be accurately predicted from first principles using the Faran model and the acoustical properties of glass.

Further complexities are introduced in our experiments with AML cells since their reflection does not increase linearly at low densities. This difference is probably due to two parameters. One is the amplitude of the reflection coefficient of the particle layer relative to the reflection coefficient of the underlying surface. The other is the phase shift between the echo from the layer of particles and the echo from the underlying surface. For the glass beads, the reflection coefficient of a single layer is much larger than the reflection coefficient from the surface underneath ($r_c = 0.221$ and 0.008, respectively, at 40 MHz). Therefore, the echo from the glass beads is largely predominant. Moreover, the phase shift is relatively small ($<\pi/9$, at 40 MHz). In this case r_c can be estimated relatively accurately by linearly subtracting the reflection coefficient of the Aqualene surface from the total reflection coefficient R_1 of the surface covered by glass beads. In the case of AML cells, the reflection coefficient of the gelatin and the reflection coefficient of a single layer of cells are similar ($r_c = 0.005$ and 0.009, respectively) and the phase shift is significant ($>\pi/4$, at 40 MHz). Consequently, the effect of the underlying surface cannot be linearly subtracted from the reflection from the AML cells, whatever the number of AML cells may be. This leads to the initial nonlinear increase of the coefficient of reflection from AML cells as a function of the number of layers. This fact has been taken into account automatically in our model, due to its recursive nature.

As an additional complication, the reflection of a single layer of AML cells has to be obtained from an experimental fit since their theoretical backscattering cross-sections calculated using properties described by Baddour *et al* (2005) yield much larger reflection coefficients than those observed in our experiment. Such a discrepancy could be caused by the difference in the local environment of cells in layers as compared to isolated cells floating in an aqueous solution.

When glass beads and AML cells accumulate with increasing surface densities, the reflection eventually attains a maximum and oscillates. This interference phenomenon is clearly demonstrated for glass beads in figure 7, which shows ripples in both the frequency and the number-of-layers dependence of the reflection coefficient. Moreover, the distances between the maxima and the minima are regular and can be predicted by the position of the zeros of the derivative of equation (9), which is the analytical formulation of our model. This suggests that the position of the peaks can be predicted from the frequency, the size of the particles and the speed of sound. Conversely, the knowledge of the interference pattern caused by layered media allows the determination of either the speed of sound or the layers' thickness.

In addition to the period of oscillation, our model also predicts the amplitude of the reflection of multiple layers from the reflection coefficient of a single layer. As shown in figures 4–6, the concordance between experimental and theoretical values for glass beads is excellent. The model also accounts for the decrease in the amplitude of the oscillation with the number of layers and the frequency. This is caused by the reduction in the contribution of deeper layers caused by the modulation by the transmission and attenuation coefficient. The damping of the oscillation is also affected by frequency-dependent attenuation.

The prediction of the model for AML cells is less accurate, especially when several layers of cells are present. However, it seems to correctly predict the maximum reflection coefficient and the number of layers required. The period is overestimated and the attenuation underestimated. The difference between prediction and measurement is possibly due to the fact that the measurements of the speed of sound and attenuation used in the model were performed in centrifuged pellets of cells which are likely to be more packed than cells left to sediment for 1 h.

The oscillations of the reflection coefficient as a function of the number of layers of AML cells are smoothed out. Although it has a perceptible trough after the first maximum, the reflection coefficient seems to stabilize after the first oscillation at a value above 0.02. This behavior could be explained by the broader size distribution of the AML cells with respect to the glass beads. After a few layers, the layers become less defined and the cells are packed randomly in the vertical direction, therefore canceling the interference phenomenon. This regime is likely to be better explained by models assuming the random position of cells such as the one developed by Hunt *et al* (2002).

The model presented here is based on the hypothesis that the maxima and minima of the reflection coefficient are caused by interferences between layers. The reflection of a single layer determines the overall amplitude of the oscillation. The real part of the phase of the wave propagating through the layer determines the period of oscillation while the imaginary part determines the damping. Rather than using the impedance of each layer, our theoretical description uses the backscattering of individual particles to calculate the reflection coefficient of layered media. In fact, the layers are seen as infinitely thin planes with a specific reflection and transmission coefficient regularly spaced within a uniform medium with a speed of sound and attenuation established by transport theories. This perspective comes from the fact that the beads, as seen by the wave, are much smaller than their geometric radius.

In some ways, this interference theory applied to layers of AML cells is similar to the description of the scattering from blood using the hybrid method (Mo and Cobbold 1992). The scattering is comprised of a fluctuation term, which originates from the pseudo-random placement of the cells over each layer, and a crystallographic term which originates from the regular spacing of each layer. Contrary to the scattering from red blood cells, however, the crystallographic contribution from layers of cells is significant because the phase shift cannot be assumed to be randomly distributed.

The model presented was applicable because, even at high surface concentrations, layers of particles still transmit a significant fraction of the incident sound, and the echo from lower layers can interfere with the echo from top layers. It is thus limited to particles with small scattering cross-sections. The total scattering cross-section of glass beads of 5.1 μm in diameter (at 30 MHz), as calculated from the Faran model (Faran 1951), is 2×10^{-13} m^2 or a hundred times smaller than the geometrical cross-section. Otherwise multiple scattering would also have to be taken into account in the interference model. This could be further investigated using highly scattering objects, such as microbubbles.

In the model, the assumption of linear plane wave propagation is used for simplicity. Experimentally, the reflection coefficient is measured as a ratio of the reflected pressure at the

fundamental between the surface covered with particles and a reference reflector. Hence, the reflection coefficient is affected by nonlinear propagation in the reflection path, which might lead to its overestimation if sufficiently high input pressures are used. For higher amplitudes or oblique incidences, the reflection coefficient should be obtained using a numerical model of wave propagation.

The interference model could be applied to explain the appearance of layered tissue such as the wall of the stomach or of arteries. It requires the reflection coefficient, the speed of sound and the attenuation of each layer independently. These values could be determined experimentally through micro-dissection of tissue into its constituent layers (Siegel *et al* 1993), the reflection of grown layers of cells on culture plates or by using models of the scattering cross-section of individual cells. Also, the interference model can predict the maximum possible reflectivity enhancement obtainable from contrast agents such as perfluorocarbon particles. Such knowledge is fundamental to optimize their use.

6. Conclusion

This study has demonstrated that the reflection coefficient of glass beads and AML cells accumulated on surfaces can be measured reproducibly. The oscillatory behavior of the reflection coefficient reveals an interference phenomenon between the different layers of particles (glass beads and cells). Although the maximum reflection coefficient was very different between the glass beads ($r_c = 0.38$) and AML cells ($r_c = 0.02$), they could both be predicted with an interference model. This interference model determines first the reflection of a single layer using the scattering cross-section of the particles and then sums the phase-shifted contribution of all the layers. The application of this model could also be inverted to determine the scattering cross-section of particles from the reflection due to a full layer. In the future, this model could be used to explain the appearance of layered tissue and predict the maximum reflectivity enhancement of contrast agents.

Acknowledgments

We thank the Canadian Institutes of Health Research, the Ontario Research and Development Challenge Fund, Visualsonics and the Terry Fox Programme of the National Cancer Institute of Canada for their funding. We also thank the laboratory of Gregory Czarnota for providing the AML cells and Ralph Baddour and Roxana Vlad for fruitful discussions.

References

Baddour R E, Sherar M D, Hunt J W, Czarnota G J and Kolios M C 2005 High-frequency ultrasound scattering from microspheres and single cells *J. Acoust. Soc. Am.* **117** 934–43

Bolondi L, Casanova P, Santi V, Caletti G, Barbara L and Labo G 1986 The sonographic appearance of the normal gastric wall: an *in vitro* study *Ultrasound Med. Biol.* **12** 991–8

Buckingham M J 1997 Theory of acoustic attenuation, dispersion, and pulse propagation in unconsolidated granual materials including marine sediments *J. Acoust. Soc. Am.* **102** 2579–96

Chivers R C and Santosa F 1986 Numerical considerations for interface reflections in medical ultrasound *Phys. Med. Biol.* **31** 819–37

Cobbold R S C 2007 *Foundations of Biomedical Ultrasound* (Oxford: Oxford University Press)

Couture O, Bevan P D, Cherin E, Cheung K, Burns P N and Foster F S 2006 A model for reflectivity enhancement due to surface bound submicrometer particles *Ultrasound Med. Biol.* **32** 1247–55

Faran J J 1951 Sound scattering by solid cylinders and spheres *J. Acoust. Soc. Am.* **23** 405–18

Hinrichen E L, Feder J and Jossang T 1990 Random packing of disks in two dimensions *Phys. Rev.* A **41** 4199–209

Hughes E R, Leighton T G, Petley G W and White P R 1999 Ultrasonic propagation in cancellous bone: a new stratified model *Ultrasound Med. Biol.* **25** 811–21

Hunt J W, Worthington A E, Xuan A, Kolios M C, Czarnota G J and Sherar M D 2002 A model based upon pseudo regular spacing of cells combined with the randomisation of the nuclei can explain the significant changes in high-frequency ultrasound signals during apoptosis *Ultrasound Med. Biol.* **28** 217–26

Insana M F, Wagner R F, Brown D G and Hall T J 1990 Describing small-scale structure in random media using pulse-echo ultrasound *J. Acoust. Soc. Am.* **87** 179–92

Lanza G M, Trousil R L, Wallace K D, Rose J H, Hall C S, Scott M J, Miller J G, Eisenberg P R, Gaffney P J and Wickline S A 1998 *In vitro* characterization of a novel, tissue-targeted ultrasonic contrast system with acoustic microscopy *J. Acoust. Soc. Am.* **104** 3665–72

Lim J H and Jeong Y M 1994 Sonography of the stomach: an in vitro study to determine the anatomic cause of inner hyperechoic and hypoechoic layers of the gastric wall *Am. J. Roentgenol.* **162** 335–8

Mo L Y and Cobbold R S C 1992 A unified approach to modeling the backscattered Doppler ultrasound from blood *IEEE Trans. Biomed. Eng.* **39** 450–61

Shung K K and Thieme G A (ed) 1993 *Ultrasonic Scattering in Biological Tissues* (Boca Raton, FL: CRC Press)

Siegel R J, Chae J S, Maurer G, Berlin M and Fishbein M C 1993 Histopathologic correlation of the three-layered intravascular ultrasound appearance of normal adult human muscular arteries *Am. Heart J.* **126** 872–8

Sleefe G E and Lele P P 1988 On estimating the number density of random scatterers from backscattered acoustic signals *Ultrasound Med. Biol.* **14** 709–27

Williams K L, Jackson D R, Thorsos E I, Tang D and Schock S G 2002 Comparison of sound speed and attenuation measured in a sandy sediment to predictions based on the bio theory of porous media *IEEE J. Ocean. Eng.* **27** 413–28